EUT EDIZIONI UNIVERSITÀ DI TRIESTE

Bollettino della ASSOCIAZIONE ITALIANA di CARTOGRAFIA **2019 (166), 4-14**

ISSN 2282-572X (online) ISSN 0044-9733 (print)
http://www.openstarts.units.it/dspace/handle/10077/9933

DOI: 10.13137/2282-572X/30185

Remote sensing image time series analysis at a pixel level. The temperature trend in Friuli Venezia Giulia from a Landsat database (1987-2016)

Telerilevamento su serie storica di immagini satellitari Landsat a livello dei pixel. L'andamento della temperatura in Friuli Venezia Giulia (1987-2016)

ANDREA FAVRETTO

Università di Trieste; afavretto@units.it

Abstract

This paper is a study on the temperature trend in Friuli-Venezia Giulia (North-East of Italy), based on a Landsat remote sensing image time series from 1987 to 2016.
The thermal bands of the Landsat carried sensors were transformed into Celsius degrees. Each image was masked in order to exclude clouds and cloud shadow effects. A regression analysis was then carried out on the image time series.
The result was a thematic map showing the distribution of the temperature trend in the study area.
The built model showed a certain temperature increase trend (given by the values of the slope parameter of each built regression line), especially in the urban and suburban areas of the study area, plus in the Alpine region and in the North of the Marano lagoon area.

Keywords

Landsat, Temperature trend, Friuli Venezia Giulia, Pixel based analysis, Remote sensing Image time series

Riassunto

Il contributo presenta uno studio sull'evoluzione della temperatura nel Friuli-Venezia Giulia, sulla base di immagini satellitari a media risoluzione spaziale. Si è lavorato su una serie storica di immagini Landsat 4, 5, 7, 8, riprese dal 1987 al 2016.
La banda termica del sensore è stata trasformata in gradi Celsius. Ogni immagine è stata mascherata dalle nuvole. È stato applicato un modello di regressione lineare alla serie storica di immagini telerilevate, a livello di ciascun pixel di ogni immagine. È stato realizzato un layer raster nel quale ciascun pixel riporta la pendenza della retta di regressione, costruita per quel pixel dalla serie storica delle immagini. In questo modo si è potuto verificare, da un punto di vista posizionale, il trend evolutivo della temperatura nell'area di studio.
Il modello sviluppato ha mostrato un sensibile incremento della temperatura nel periodo considerato, evidenziato peraltro dai valori della pendenza della retta di regressione costruita. Tale incremento è stato più evidente nelle aree urbane e suburbane dell'area di studio, più l'area alpina e la zona a Nord della laguna di Marano.

Parole chiave

Landsat, Trend temperature, Friuli Venezia Giulia, Analisi basata sui pixel, Serie storica immagini telerilevate

1. Introduction

It is well-known that Remote Sensing methods are based on the detection of the ElectroMagnetic Radiation (EMR) by the sensors on a remote platform. The Land Surface Temperature (LST) can be directly related to the physical temperature of the land surface[1] and therefore LST can be estimated from the EMR emitted in the Thermal InfraRed (TIR) spectral region (between 8 and 15 μm). Satellite TIR sensors measure the Top Of Atmosphere (TOA) radiance, which includes "upwelling radiance emitted from the ground, upwelling radiance from the atmosphere, and the downwelling radiance emitted by the atmosphere and reflected from the ground" (Tomlinson *et Al.*, 2011). TOA is converted to LST by correcting its three main effects: "atmospheric attenuation, angular effects and spectral emissivity values at the surface" (Tomlinson, op. cit.).

A well-known drawback to the LST estimation using the TIR techniques is made up of clouds. Clouds completely block emissions from the land surface. This means "that spaceborne TIR radiometers give no information about the land surface below the clouds and instead reflect the temperature and emissivity of the clouds" (Holmes *et Al.*, 2016).

For this reason, remote sensed data very often come with the so called "mask layers". These layers record the image pixels classified as cloud (and cloud shadow) by the data provider. If Landsat data are used (as in this case, see the next "Database" paragraph), a Pixel Quality Assessment band is available together with each image. In this layer the user can find the position of clouds, cloud shadows and snow/ice on the Landsat image (see USGS (a) and (b), 2018). Clouds, cloud shadows and snow/ice flags are derived from the CFMask algorithm (see, among others, Foga *et Al.*, 2017).

Analyses of remote sensing image time series have been performed for a long time on broad-scale sensor, such for instance AVHRR, MERIS, MODIS (Hostert *et Al.* 2015). After the 2008 USGS[2] free data policy adoption for the whole Landsat archive, time series image analyses became a real new research frontier (Weng, 2018). So remote sensing analyses on image time series at a fine-scale (Landsat) are easier since 2008. In this way Planet Earth and the way the same is changing can be studied at no cost (Woodcock *et Al.*, 2008). Traditional analyses such as multi-temporal image classification can be easily replaced with pixel based analyses to derive metrics for mapping or monitoring and "such metrics may include linear or nonlinear trends, amplitude, phase or break points" (Hostert *et Al.*, op. cit.).

With regards to the urban and suburban areas, the relation between surface temperatures and vegetation density was deeply studied also with remote sensing methods. Using Landsat TM imagery, Kawashima (1994) observed that: "The degree of vegetation effect on surface temperature depends on the difference between the percentage of buildings area and that of forests area". Boukhabla *et Al.* (2012) highlighted that in the urban areas "The parks contribute significantly to the reduction of air temperature" with the three specific effects of vegetation shade, evotraspiration and natural ventilation. Considering remote sensing methods, the relationship between NDVI (Normalized Difference Vegetation Index) and temperature was long recognized. NDVI is considered one of the most important indicators of the urban climate (Gallo *et al.*, 1993; among the most recent: Zhang *et al.*, 2010; Zeng *et al.*, 2010; Keramitsoglou *et al.*, 2011). A negative correlation between NDVI and LST has been indicated (Deng *et Al.*, 2018; Yue *et Al.*, 2007; Sun *et Al.*, 2007).

With regard to the Trieste Province and using remote sensing methods, two studies were carried out in order to study the sprawl of Trieste town towards its rural areas. The first one (Favretto *et Al.*, 2003) tried to measure the loss of rural land from 1975 to 1999 by applying NDVI to four different Landsat images. The analysis showed a significant loss of green areas (11.4 sq. km out of a total of 212 sq. km) in the Trieste Province during the considered period. A second study (Favretto,

1 These kind of studies date back to the 1970s, see for instance: McMillin, 1975.

2 United States Geological Survey is the largest water, earth, and biological science and civilian mapping agency in the USA (https://www.usgs.gov/). Landsat project is a joint effort of USGS and National Aeronautics and Space Administration (NASA). "The USGS then assumes ownership and operation of the satellites, in addition to managing all ground reception, data archiving, product generation, and data distribution" (see USGS, 2012).

ISSN 2282-572X (online)
ISSN 0044-9733 (print)

2018) aimed at monitoring the main vegetation changes in the Trieste province between 2000 and 2017. Nine different Landsat images were elaborated in order to calculate EVI (Enhanced Vegetation Index). While the less vegetated classes ("Built"/"Bare soils"/"Grass") remained quite unchanged in the considered period, the "Bush" and "Wood" classes registered the most significant changes. In fact, the first fell from 45.9 to 19.5 sq. km while the second increased from 67.5 to 75.6 sq. km.

We think that the vegetation dynamics in the Trieste Province could help explaining the registered increment of the local temperature. In the near future, we will therefore apply the same methodologies to the Udine, Pordenone and the Alpine areas to verify the local vegetation evolution.

This paper studies the temperature trend in Friuli Venezia Giulia (North-East of Italy)[3]. The analysis is carried on a Landsat image time series, from 1987 to 2016. All the satellite images were taken in the July/August months in order to ensure the maximum consistency among the scenes. In order to highlight a linear trend, we ran a regression analysis on each image time series pixel. So we produced a thematic map showing the estimated slope distribution in the study area.

The paper is organised as follows: first the used satellite image database is presented. Next, the methods used in the study are introduced (in the "Remotely sensed imagery elaboration" paragraph). The paper closes with the main results, followed by a short conclusion.

2. Database

The used remotely sensed images are shown in Table 1.

All images have been released by USGS[4] as Climate Data Records (CDR). CDR are "higher-level Landsat data products to support land surface change study" (USGS, 2017), and also include the surface reflectance (SR)[5].

The used TM images were atmospherically corrected to SR using the Landsat Ecosystem Disturbance Adaptive Processing System (LEDAPS) specialised software[6] (see USGS, 2016).

The used OLI images were atmospherically corrected to SR using the Landsat Surface Reflectance Code (LaSRC) algorithm. LaSRC has replaced the previous Landsat 8 Surface Reflectance (L8SR, on June 2016). The main differences between the LEDAPS and LaSRC algorithms can be seen on USGS, 2016. One important difference is the data sources for the atmospheric composition, which, in the case of LEDAPS, are from the National Centres for Environmental Prediction (NCEP – http://www.ncep.noaa.gov/), and in the case of LaSRC, are MODIS remotely sensed data.

With regard to thermal channels, the Top of Atmosphere Brightness Temperature (TOABT) output from Landsat 7 ETM+, Landsat 5 TM and Landsat 4 TM (converted to Kelvin), are delivered with the thermal Band 6.

3 Friuli-Venzia Giulia (FVG) is an Italian special administrative region, created in 1948 as the result of the combination of two different geographical entities. Its closeness to Austria and Slovenia gave birth to a mixed ethnolinguistic reality. FVG territory is mountainous (43%), flat (38%) and hilly (19%). Carniche and Giulie Alps are in the Northern territories of the region while the Padana plain occupies its Southern areas. Trieste, the main city, is surrounded by the Karst plateau. Next to the Friuli plain are the Grado and Marano lagoons while the Gulf of Trieste shows a high and rocky coast (to deepen the physical geographic features of FVG, see the tabs of landscape areas in the recently approved regional landscaping plan – PPR 2018 – https://www.regione.fvg.it/rafvg/cms/RAFVG/ambiente-territorio/pianificazione-gestione-territorio/FOGLIA21/#id1; a socio-economic analysis of FVG can be found in: Zaccomer, 2019). The other main towns in FVG are: Udine, Pordenone, Gorizia and Monfalcone.
Corn crops, wheat, vineyards and sugar beet grow in the Friulana plain. Breeding of swine and fishing complete the FVG agro-food sector. Petrochemical plants and shipyard industries are located mainly in the Trieste and Monfalcone areas. Udine guests small and medium-sized firms in the mechanical, food, wood, furniture and knives sectors. The engineering sector is located in Pordenone.

4 See: ESPA (Earth Resources Observation and Science /EROS Center Science Processing Architecture) on demand interface (https://espa.cr.usgs.gov/).

5 SR is the satellite derived Top of Atmosphere reflectance (TOA) "corrected for the temporally, spatially and spectrally varying scattering and absorbing effects of atmospheric gases and aerosols" (Vermote *et Al.*, 2016).

6 LEDAPS applies Moderate Resolution Imaging Spectroradiometer (MODIS) atmospheric correction software to Level-1 data products (see the standard parameters in: https://landsat.usgs.gov/landsat-processing-details). All the environmental variables external to the satellite scene (for instance: water vapor, ozone, aerosol optical thickness, digital elevation, etc.) are used, together with Landsat image and input to the Second Simulation of a Satellite Signal in the Solar Spectrum (6S, see Vermote *et Al.*, 1997) radiative transfer model to generate all the higher-level products.

ISSN 2282-572X (online)
ISSN 0044-9733 (print)

TABLE 1 – The remotely sensed database. TM: Thematic mapper; ETM+: Enhanced Thematic Mapper; OLI: Operational Land Imager; CRS: Coordinate Reference System; Sun elevation: "angle in degrees for the image centre location at the image centre acquisition time" (see: Landsat Data Dictionary – Sun Elevation – USGS https://lta.cr.usgs.gov/DD/landsat_dictionary.html#image_quality_landsat_8-9)

Acquired on	Satellite	Sensor	Path/Row	Quality	Sun elev.	CRS
1987-07-20	Landsat 5	TM	191/028	7	55.55	WGS84/UTM/33
1991-07-23	Landsat 4	TM	191/028	9	53.83	WGS84/UTM/33
1993-08-05	Landsat 5	TM	191/028	7	52.08	WGS84/UTM/33
1994-07-23	Landsat 5	TM	191/028	7	53.99	WGS84/UTM/33
2000-08-16	Landsat 7	ETM+	191/028	9	52.76	WGS84/UTM/33
2001-07-26	Landsat 5	TM	191/028	9	56.37	WGS84/UTM/33
2003-08-17	Landsat 5	TM	191/028	9	51.16	WGS84/UTM/33
2004-07-18	Landsat 5	TM	191/028	9	57.98	WGS84/UTM/33
2007-07-27	Landsat 5	TM	191/028	9	57.85	WGS84/UTM/33
2009-07-16	Landsat 5	TM	191/028	9	59.12	WGS84/UTM/33
2011-08-23	Landsat 5	TM	191/028	9	50.79	WGS84/UTM/33
2013-07-27	Landsat 8	OLI	191/028	9	58.67	WGS84/UTM/33
2015-07-17	Landsat 8	OLI	191/028	9	60.30	WGS84/UTM/33
2016-08-04	Landsat 8	OLI	191/028	9	56.67	WGS84/UTM/33

SOURCE: Landsat data elaboration

In the Landsat 8 case, USGS delivers the TOABT (also in Kelvin), derived by the TOA radiance. TOA radiance is collected by the Thermal Infrared Sensor (TIRS) with two spectral bands (10 and 11) for the wavelength covered by a single band on the previous TM and ETM+ sensors (see: https://landsat.usgs.gov/landsat-8). USGS recommends "that users refrain from relying on band 11 data in quantitative analysis of the TIRS data due to the larger calibration uncertainty associated with this band" (see: https://landsat.usgs.gov/using-usgs-landsat-8-product) .

All the images were: "L1T" Data Type. This means that they were orthorectified using Ground Control Points (GCP) and a Digital Elevation Model (DEM) to correct for relief displacement (see: https://landsat.usgs.gov/landsat-processing-details).

We tried to gather the largest possible number of images since the 1980's, according to the image conditions (see the upper Image quality parameters[7]) and the available 191/28 (path/row) scenes at USGS.

The image time series has been collected in order to ensure maximum consistency among images.

As the metadata for each image shows (see Table 1), all the chosen Landsat images were taken during the same season (summer) and they were acquired over 5 weeks (between the 16th July and the 23th August). This fact ensured an enough close sun elevation value for each image (between 50.79 and 59.12 degrees).

7 The image quality (values from -1 to 9) is based on the number and distribution of bad scans or equivalent bad scans in a scene (see: Landsat Data Dictionary – Image Quality – USGS https://lta.cr.usgs.gov/DD/landsat_dictionary.html#image_quality_landsat_8-9).

ISSN 2282-572X (online)
ISSN 0044-9733 (print)

3. Satellite imagery elaboration

First of all, we transformed each thermal band from degrees Kelvin to degrees Celsius.

We decided not to calculate the LST for each image but to elaborate directly the USGS given TOABT because our study is a trend analysis. Our aim is to quantify the temperature increment or decrement in the study area with a dimensionless parameter such as the regression line slope of each pixel in the image series.

Then we isolated the FVG territory in each satellite scene by masking each image with a vector layer of the Italian Region administrative borders. The 191/28 path/row of the Landsat project covers almost the entire territory (only a small part of the western Province of Pordenone town is not included). Not only: if we check the FVG territory included in the 191/28 path/row, we can see that this path/row has slightly moved over time.

In the Fig. 1 you can respectively see, from bottom to top: Landsat 5 (1991) thermal band 6 (visualized in grey); Landsat 8 (2016) thermal band 10 (visualized in green); vector layer of the FVG region (in red). It is easy to see that the two satellite scenes are slightly different in their position (and in their dimensions). In order to

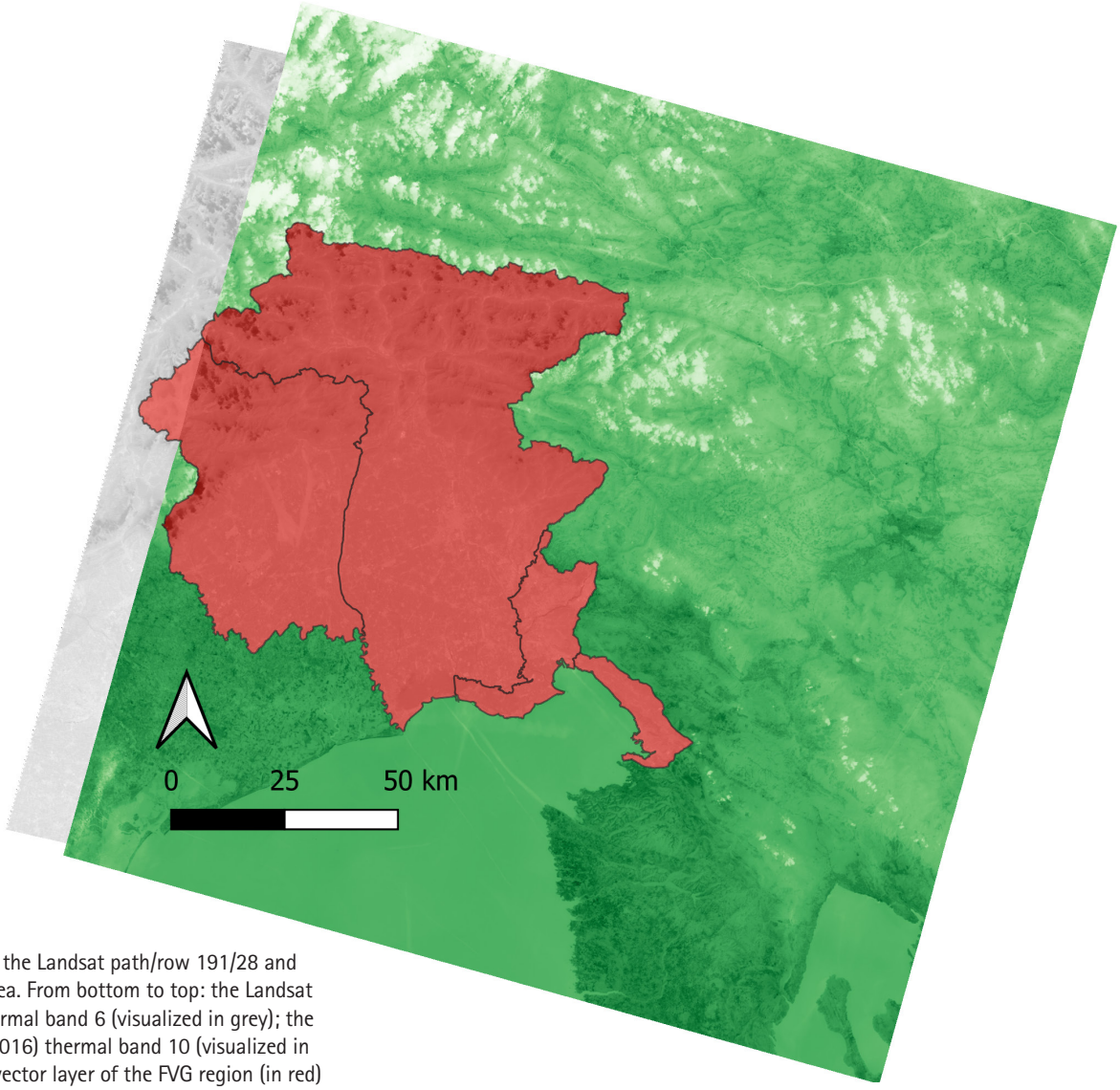

FIGURE 1
Evolution of the Landsat path/row 191/28 and the study area. From bottom to top: the Landsat 5 (1991) thermal band 6 (visualized in grey); the Landsat 8 (2016) thermal band 10 (visualized in green); the vector layer of the FVG region (in red)

ISSN 2282-572X (online)
ISSN 0044-9733 (print)

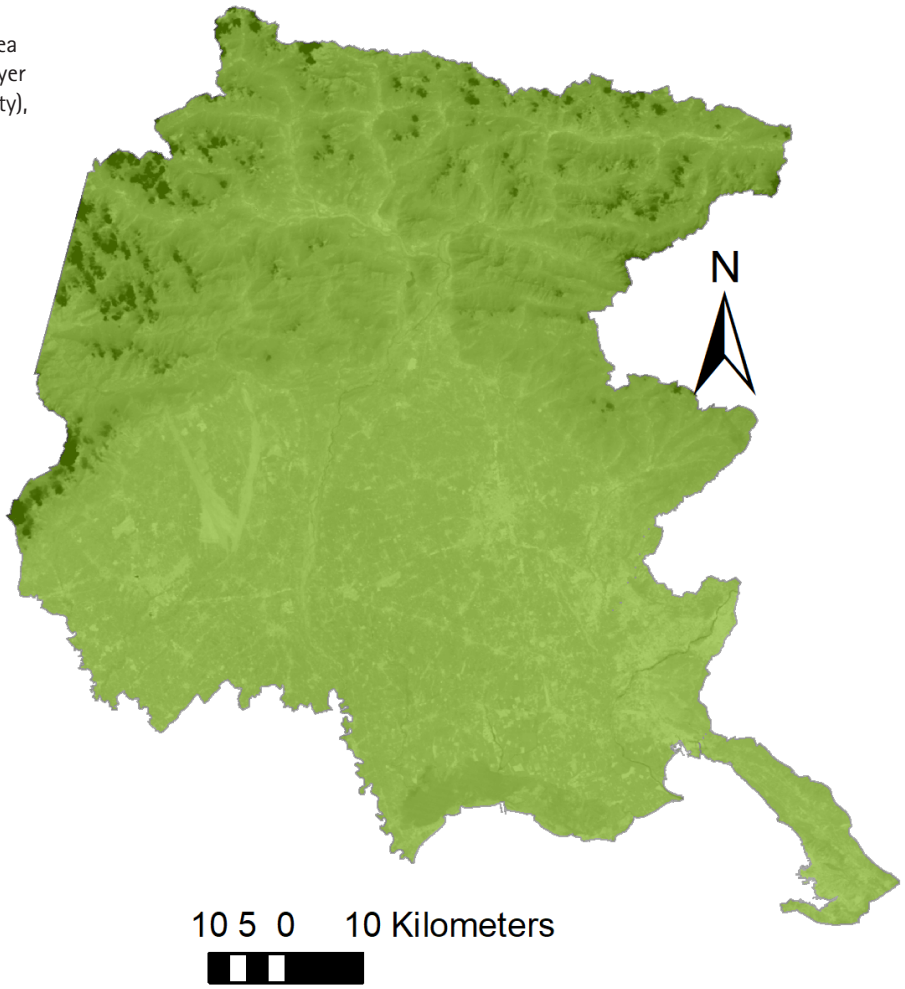

FIGURE 2
The Friuli Venezia Giulia (FVG) smaller area on the Landsat scenes. The FVG vector layer in the figure (in green, with a 40% opacity), is overlaid to the masked 2001 Landsat 5 band 6 image of the time series.

have the same part of territory in each scene of the time series, we used a vector layer with a smaller FVG Region area in order to mask the same area in all the images of our time series. Fig. 2 shows the "smaller area" version of the FVG vector layer. The vector layer in the figure (in green, with a 40% opacity), is overlaid to the masked 2001 Landsat 5 band 6 image of our time series.

It is well known that cloud presence in satellite scenes is an important factor that can preclude meaningful observations at reflective wavelengths (Zhang *et Al.*, 2018).

The Landsat 4-7 and 8 Collection 1-L1TP products include a per-pixel quality band (the "pixel_qa" tif layers). In these layers, information about the presence of pixel labeled as "cloud", "cloud shadow", "cirrus", or "snow" are available. These information flags are derived from the CFMask algorithm (see: USGS, 2018 and Foga *et Al.*, 2017).

Using the "pixel_qa" tif layers we discarded all the pixel observations (of the FVG masked Landsat layers), labelled as "cloud", "cloud shadow", "cirrus", or "snow". As an instance, Fig. 3 shows the 2001 Landsat 5 band 6, masked with the FVG vector layer and cleaned from the cloud effects in the original scene (the layer is displayed in shades of red: low Celsius degrees-light red; higher Celsius degrees-dark red).

ISSN 2282-572X (online)
ISSN 0044-9733 (print)

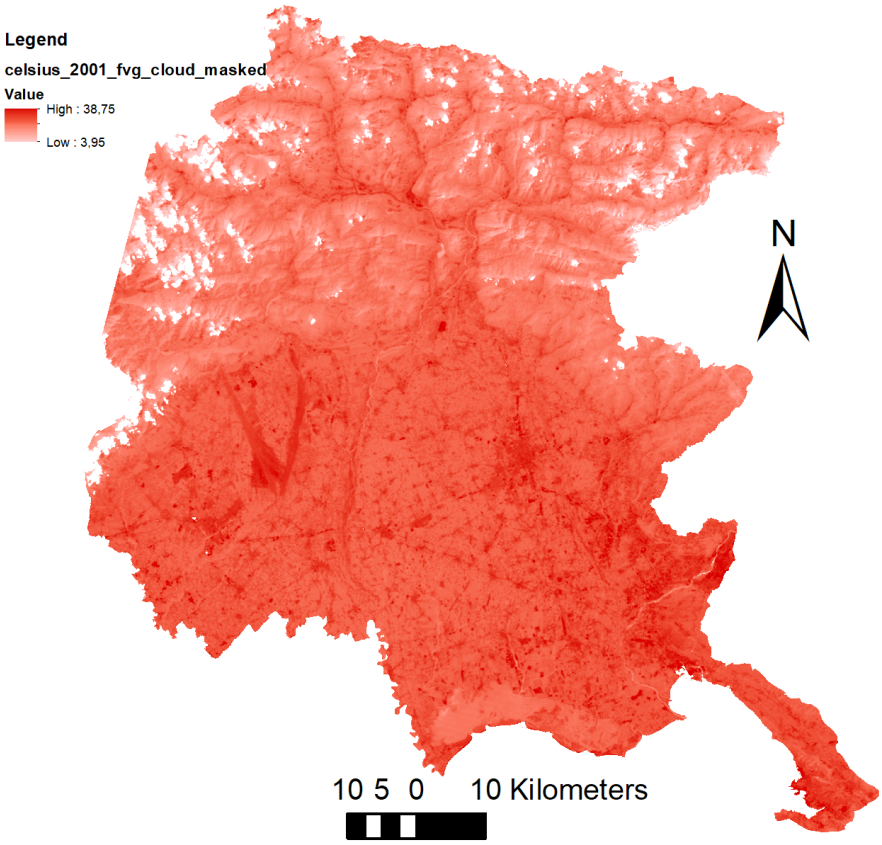

FIGURE 3
Cleaning the cloud and cloud shadow effect in the image time series. The 2001 Landsat 5 band 6, masked with the FVG vector layer and cleaned from the cloud effects in the original scene (the layer is displayed in shades of red: low Celsius degrees-light red; higher Celsius degrees-dark red).

Then we ran a regression analysis on our transformed time series. We chose a linear model

$$Y = aX + b$$

because of its simplicity and because it eases the result interpretation. We also calculated the coefficient of determination (R-squared – R^2) for our model.

Figg. 4 and 5 show the results of the applied procedure to the image time series.

Fig. 4 shows the slope distribution ("a" parameter) of the straight-line equation above. We added some place names on the thematic map in order to ease the discussion on the results (see the "Results" paragraph). The slope variability is between -1 and +1. A positive slope indicates an increment in temperature (calculated from the regression of this pixel in the time series), while negative slopes the contrary. The no-data areas of the image are the discarded pixels in at least one of the time series images. The slope values were classified with the natural breaks algorithm in six class intervals (Jenks classification, see: de Smith, 2009). In the classified map we tried to enhance the model results with different colours. The areas with a temperature decrease are blue. Unchanged temperature areas are green while the colours from yellow to light brown indicate different levels of temperature increase areas.

Fig. 5 shows the distribution of the R^2 coefficient for each pixel fitted line. The R^2 variability is between 0 and +1 and represents the scatter around the regression line (a low R^2 value indicates a low explanation of the response variable variation around its mean while a high R^2 value the contrary). In order to enhance their appearance, R^2 values were stretched using the percent clip method (values range: 0 to 0.96).

ISSN 2282-572X (online)
ISSN 0044-9733 (print)

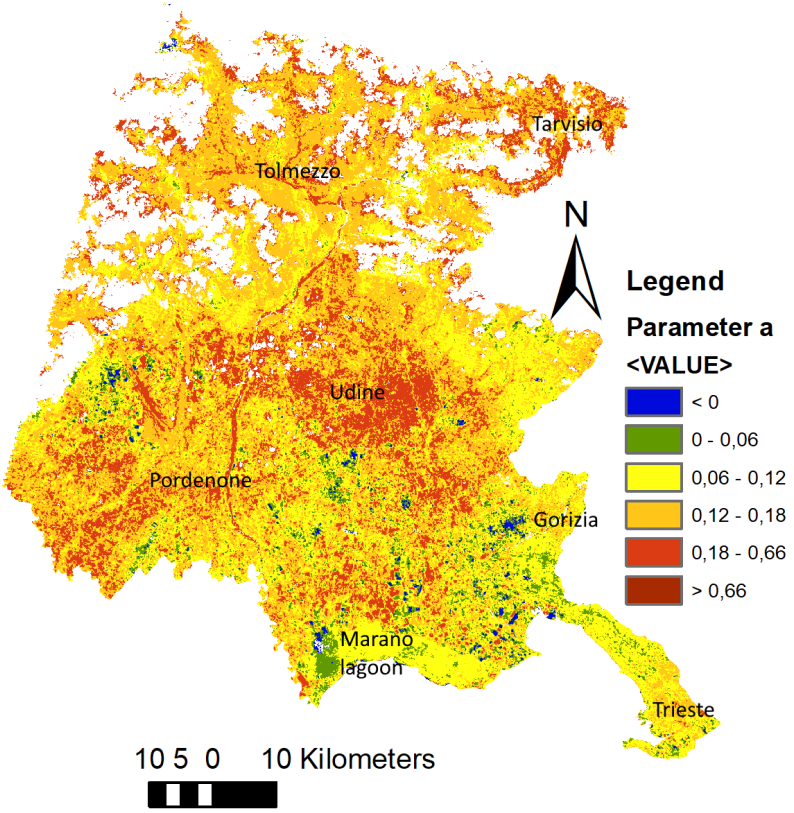

FIGURE 4
Results. The distribution of the slope ("a" parameter) of the straight-line equation in the study area The slope values were classified with the natural breaks algorithm in six class intervals. A positive slope indicates an increment in temperature while negative slopes the contrary.

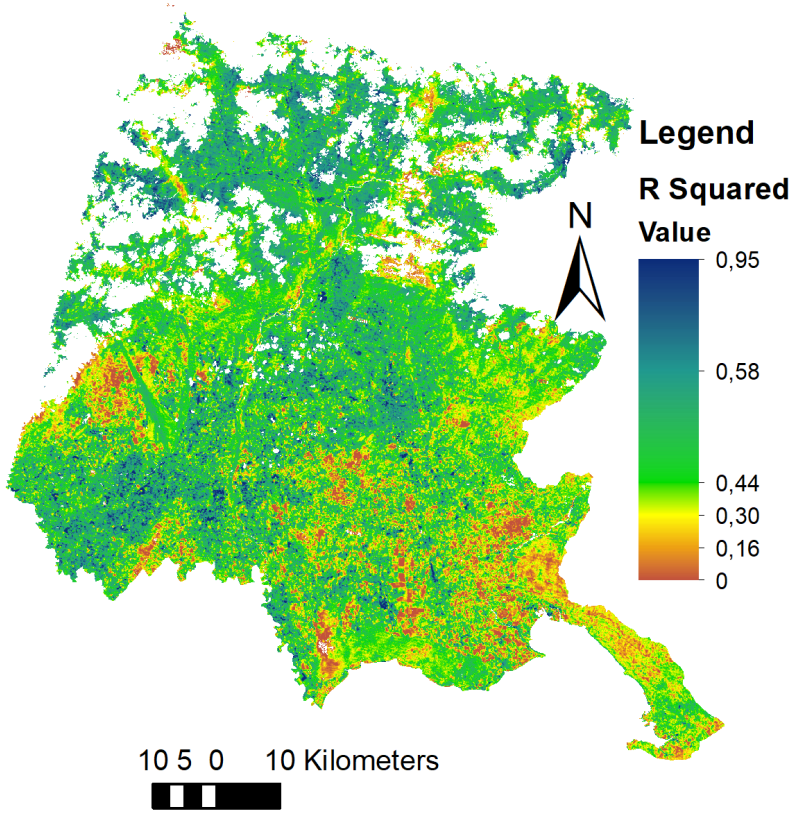

FIGURE 5
The distribution of the R^2 coefficient for each pixel fitted line in the study area. A low R^2 value indicates a low explanation of the response variable variation around its mean while a high R^2 value the contrary.

ISSN 2282-572X (online)
ISSN 0044-9733 (print)

4. Results

Fig. 4 represents a thematic map showing the slope distribution of a linear trend along the time series values in the study area. Observing the figure, we can see that in the study area the positive values of the "a" parameter are clearly predominant in comparison with the negative ones. More precisely, we can observe that data mainly fall in the "0.12-0.66" range (orange and red areas in the map). The Northern areas (the Alpine Region) are mainly orange/red while the areas around the Udine and Pordenone towns are red/orange. Another red/orange area is located in the South-East of the study area (near the Marano Lagoon). Finally, the Trieste municipality area results yellow/orange.

Fig. 5 is a thematic map showing the R^2 distribution in the study area. R^2 values are connected to the linear trend along the time series values. Observing the two figures, we can see that the same areas with the highest slope values (the red and orange ones in fig. 4), seem to be the areas with the higher R^2 values in fig. 5 map (the light green and dark green areas). This fact could suggest that the fitted model is most effective when depicting a higher temperature increase rather than a lower/stable/decrease one.

5. Conclusion

We studied a remote sensed image time series at a pixel level in order to highlight the temperature evolution in Friuli-Venezia Giulia during the 1987-2016 period. We used 14 Landsat images at this aim (TM, ETM+ and TIRS sensors). We considered only summer images (taken on July and August) and also images with a cloud cover less than 20%. The reduced number of images is due to the data availability in the USGS servers and to the chosen temporal and quality constraints[8]. We used the TOABT instead of the LST pixel values because we wanted to make a trend analysis and therefore we did not need to consider the precise land temperature.

We fitted a linear model to each time series pixel value and we created the slope distribution map in the study area. In order to validate our linear model, we also made R^2 values distribution map in the study area.

We observed a certain temperature increase trend (given by the highest values of the a parameter in our model), especially in the urban and suburban areas of the study area, plus in the Alpine Region and in the North of the Marano Lagoon area (see the thematic map in Fig. 4). We think that these results could be connected to the economic activities around and inside the main towns of the study area. We think that the green management could also be considered in order to explain the temperature trend (see Trieste vegetation studies in the Introduction paragraph). Our hypothesis is based on some previous analyses in the Trieste Province territory. In the future, we mean to study the vegetation trend in the Alpine Region, in the Udine and Pordenone Provinces in order to verify our assumption.

Acknowledgments
Landsat remote sensed imagery courtesy of the U.S. Geological Survey Earth Resources Observation and Science Center.

8 As Hostert *et Al.* wrote (2015), sometimes the ideal time series approach cannot be persuaded due to data constraints (reduced availability of historical remote sensed Landsat images outside the USA).

ISSN 2282-572X (online)
ISSN 0044-9733 (print)

References

Boukhabla M., Alkama D. (2012), "Impact of vegetation on thermal conditions outside, Thermal modeling of urban microclimate, Case study: the street of the republic, Biskra", *Energy Procedia*, 18, pp. 73-84.

de Smith M. J., Goodchild M. F., Longley P. A. (2009), *Geospatial Analysis – A Comprehensive Guide to Principles, Techniques and Software Tools*, 3rd edition; Matador, Leicester.

Deng Y., Wang S., Bai X., Tian Y., Wu L., Xiao J., CCChen F., Qian Q., "Relationship among land surface temperature and LUCC, NDVI in typical karst area", *Scientific Reports*, 8, n. 641, 2018, 2045-2322.

Favretto A., Jürgens C. (2003), "Change detection techniques applied on satellite imagery in order to delineate urban sprawl evolution in Trieste Province (North East of Italy) between 1975 and 1999", *The International Archives of the Photogrammetry, Remote Sensing and spatial information changes*, XXXIV-7/W9.

Favretto A. (2018), "Checking vegetation changes with Remote Sensing: the case of the Trieste province (North-East of Italy)", *Remote Sensing Applications: Society and Environment*, 11, pp. 1-10.

Foga S., Scaramuzza P. L., Guo S., Zhu Z., Dilley Jr R. D., Beckmann T., Schmidt G. L., Dwyer J. L., Hughes M. J., Laue B. (2017), "Cloud detection algorithm comparison and validation for operational Landsat data products", *Remote Sensing of Environment* 194, pp. 379–390.

Gallo K. P., McNab A. L., Karl, T. R., Brown J. F., Hood J. J., Tarpley J. D. (1993), "The use of a vegetation index for assessment of the urban heat island effect", *International Journal of Remote Sensing*, Vol. 14/11, pp. 2223-2230.

Holmes T. R. H., Hain C. R., Anderson M. C., Crow W. T. (2016), "Cloud tolerance of remote-sensing technologies to measure land surface temperature", *Hydrol. Earth Syst. Sci.*, 20, pp. 3263–3275.

Hostert P., Griffiths P., van der Linden, Pflugmacher D. (2015), *Time Series Analyses in a New Era of Optical Satellite Data*, in: Kuenzer C. *et Al.* (eds.), *Remote sensing Time Series*, Springer.

Kawashima S. (1994), "Relation between vegetation, surface temperature, and surface composition in the Tokyo region during winter", *Remote Sensing of Environment*, Vol. 50/1, pp 52-60.

Keramitsoglou I., Kiranoudis C. T., Ceriola G., Weng Q., Rajasekar U. (2011), "Identification and analysis of urban surface temperature patterns in Greater Athens, Greece, using MODIS imagery", *Remote Sensing of Environment*, 115, pp. 3080-3090.

McMillin L. M. (1975), "Estimation of sea surface temperature from two infrared window measurements with different absorptions", *Journal of Geophysical Research*, 80, pp. 5113-5117.

Sun D., Kafatos M. (2007), "Note on the NDVI-LST relationship and the use of temperature-related drought indices over North America", *Geophysical Research Letters*, Vol. 34, L24406, pp. 1-4.

Tomlinson C. J., Chapman L., Thornes J. E., Baker C. (2011), "Remote sensing land surface temperature for meteorology and climatology: a review", *Meteorological Applications*, 18, pp. 296-306.

USGS (2012), *Landsat – Earth Observation Satellites*, https://pubs.usgs.gov/fs/2015/3081/fs20153081.pdf

USGS (2016), *Landsat Surface Reflectance-Derived Spectral Indices Product Guide*, Version 3.3, December.

USGS (2017), *Earth Resource Observation and Science (EROS) Center Science Processing Architecture (ESPA) on Demand Interface*, Version 3.7, January.

USGS (a) (2018), *Landsat 8 Surface Reflectance Code (LASRC) Product Guide*, December.

USGS (b) (2018), *Landsat 4-7 Surface Reflectance (LEDAPS) Product Guide*, December.

ISSN 2282-572X (online)
ISSN 0044-9733 (print)

Vermote E. F., Tanr D., Deuz J. L., Herman M., Morcrette J. J. (1997), "Second Simulation of the Satellite Signal in the Solar Spectrum, 6S: An Overview", *IEEE Transactions on Geoscience and Remote Sensing*, Vol. 35, N. 3, pp. 675-686.

Vermote E., Justice C., Claverie M., Franc B. (2016), "Preliminary analysis of the performance of the Landsat 8/ OLI land surface reflectance product", *Remote Sensing of Environment*, 185, pp. 46-56.

Weng Q. (2018), *Remote Sensing Time Series Image Processing*, CRC Press.

Woodcock C.E., Allen R., Anderson M., Belward A., Bindschadler R., Cohen W., Gao F., Goward S.N., Helder D., Helmer E., Nemani R., Oreopoulos L., Schott J., Thenkabail P.S., Vermote E.F., Vogelmann J., Wulder M.A., Wynne R. (2008), "Free access to Landsat imagery", *Science* 320/5879, pp. 1011-1012.

Yue W., Xu J., Tan W., Xu L. (2007), "The relationship between land surface temperature and NDVI with remote sensing: application to Shanghai Landsat 7 ETM+ data", *International Journal of Remote sensing,* Vol. 28, Issue 15, pp. 3205-3226.

Zaccomer G. P. (2019), *L'analisi territoriale socio-economica in ambito paesaggistico*, Forum, Udine.

Zeng Y., Huang W., Zhan F. B., Zhang H., Liu H. (2010), "Study on the urban heat island effects and its relationship with surface biophysical characteristics using MODIS imageries", *Geo-spatial Information Science*, Vol. 13, n. 1, pp. 1-7.

Zhang H. K., Roy D. P., Yan L., Li Z., Huang H., Vermote E., Skakun S., Roger J. (2018), "Characterization of Sentinel-2A and Landsat-8 top of atmosphere, surface, and nadir BRDF adjusted reflectance and NDVI differences", *Remote Sensing of Environment*, 215, pp. 482–494.

Zhang X. X., Wu P. F., Chen B. (2010), "Relationship between vegetation greenness and urban heat island effect in Beijing City of China", *Procedia Environmental Sciences*, 2, pp. 1438-1450.

ISSN 2282-572X (online)
ISSN 0044-9733 (print)